ADVANCES IN GEOMATICS

VOLUME 03 • ISSUE 01 • OCTOBER 2025
e-ISSN: 3023-4980

ORIGINAL ARTICLE

Submission: 18/07/2025
Accepted: 19/10/2025

EFFECT OF URBAN GROWTH ON LAND SURFACE TEMPERATURE AND MITIGATION STRATEGIES: A CASE STUDY OF KATHMANDU VALLEY

Sushil SUBEDI[1]*, Rojina Thapa MAGAR[1], Bhuwan Singh BISHT[2], Subash GHIMIRE[1]

[1] Department of Geomatics Engineering, Kathmandu University, Nepal.

[2] Land Management Training Center, Government of Nepal, Nepal.

* Corresponding Author: S. Subedi, subedisushant2057@gmail.com 0009-0007-3980-5948

ABSTRACT

The rapid increase in urban population has intensified the demand for infrastructure, resulting in the conversion of natural surfaces, particularly vegetation, into built-up areas. Such non-vegetated surfaces absorb and store more heat, contributing to higher land surface temperatures. This change in land cover is seen to increase the land surface temperature. Kathmandu has experienced rapid urban growth over the past few decades. Recently, Kathmandu has been identified as being on the verge of climate change, especially in the context of urban warming. This study has incorporated remotely sensed Landsat data, utilizing remote sensing techniques, to effectively quantify the spatial extent of urban growth and its impact on land surface temperature in Kathmandu Valley, Nepal. In this research, we employed supervised classification and change detection to identify the spatial trends of land-use and land-cover change. After that, we obtained the spatial pattern of LST using the thermal band of Landsat images. Based on our analysis, we found that the urban area increased by 13% during the period from 2013 to 2019. The surface temperatures were greater for bare soil and urban land use types. The land surface temperature ranges obtained were -3.270°C to 36.460°C in 2013, -1.910°C to 27.030°C in 2016, and 13.260°C to 40.840°C in 2019. To mitigate urban warming, strategies such as expanding urban forestry, adopting reflective building materials, and promoting sustainable urban planning are recommended for Kathmandu Valley.

Keywords: Land Surface Temperature, Landsat, Urban Growth, Urban Warming.

Cited As:

Subedi, S., Magar, R. T., Bisht, B. S. & Ghimire, S. (2025). Effect of urban growth on land surface temperature and mitigation strategies: A Case Study of Kathmandu Valley, Advances in Geomatics, 3(1), 38-54. https://doi.org/10.5281/zenodo.18087219

INTRODUCTION

Urban population growth increases the need for infrastructure, resulting in the loss of vegetation and its replacement with heat-absorbing built surfaces. This change in land cover results in an increase in land surface temperature. Nepal is one of the ten least urbanized countries in the world (Joshi, 2023). However, it is also one of the top ten fastest urbanizing countries. In 2014, the level of urbanization was 18.2%, with an urban population of 5,130,000, and a rate of urbanization of 3% (Timsina et al., 2020). Between 1978 and 2000 A.D., studies in the Kathmandu Valley found a growth rate of approximately 450% in urban areas. Additionally, the temperature in the Kathmandu Valley has been recorded as 30 °C in 2005, 31 °C in 2012, and 35 °C in 2015 (Ishtiaque et al., 2017).

Land surface temperature means the skin temperature of the surface. It depends on isolation and the nature of the surface or object material. Generally, water bodies, vegetative areas, and wet soil are cooler than bare soil, sand, metal, and built-up areas. Therefore, a positive relationship exists between LST and urbanisation (K.C. & Shepherd, 2015). Satellite-based LST can be determined from thermal emission at wavelengths in either infrared or microwave, which are "atmospheric windows". However, many uncertainties are involved in retrieving LST from radiance, which is directly measured by sensors onboard. Thermal infrared (TIR)-based LST retrievals are less uncertain than microwave-based ones because of the smaller range of variation of surface emissivity in the TIR domain and the stronger dependence of the radiance on temperature (Hulley et al., 2019).

Thus, urban growth has been identified as a critical process in the valley. It has led to population influx, environmental deterioration, urban fragmentation, haphazard landscape development, stress on ecosystem structure, and alteration of land use patterns (Akher & Chattopadhyay, 2017). According to UN-HABITAT (2015), Kathmandu is vulnerable to the impact of climate change. Therefore, this research claims to investigate the effect of urban growth on land surface temperature in the valley, since LST is an essential factor controlling urban climate (Kathmandu Valley, Nepal: Climate Change Vulnerability Assessment (Inu Pradhan Salike, 2015)

The main objective of this study is to quantify the spatial extent of urban growth, assess its influence on land surface temperature patterns, and examine temporal changes in thermal behaviour across the Kathmandu Valley. Additionally, the study aims to provide evidence-based insights to support sustainable urban planning and climate-responsive strategies.

1. MATERIALS AND METHODS

1.1 Study Area

The study area is Kathmandu Valley of Nepal, which is in the Latitude range of 27°34'33"N to 27°49'4" N and the Longitude range of 85° 11' 19" E to 85° 34' 57" E as shown in Figure 1. The Kathmandu

Valley comprises the districts of Kathmandu, Lalitpur, and Bhaktapur. The average elevation is 1300 meters above mean sea level (Thapa & Murayama, 2012). It is surrounded by four high hills: Shivpuri in the northwest, Chandragiri in the southwest, Nagarjun in the northeast, and Phulchoki in the southeast. Their altitude ranges from 1500 m. to 2800 m (Bhattarai et al., 2017).

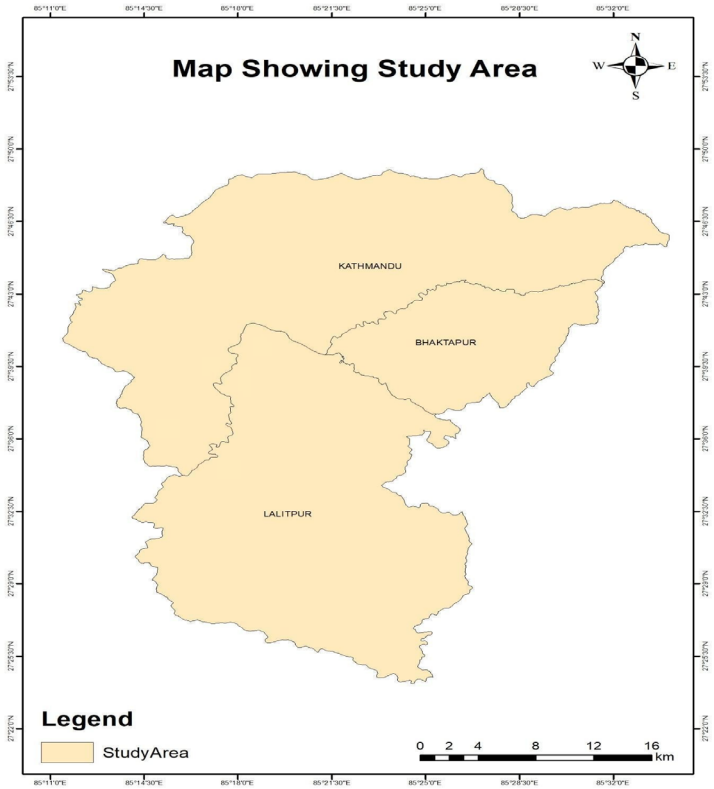

Figure 1. Study Area.

This valley was selected for this research due to its status as a rapidly urbanizing region experiencing significant landscape transformation, which provides a critical context for analyzing urban thermal impacts (Rimal et al., 2018).

1.2 Workflow

The overall workflow adopted for analyzing land surface temperature (LST) and urban growth in Kathmandu Valley is shown in Figure 2. The process begins with the acquisition of Landsat images for the years 2013, 2016, and 2019, followed by preprocessing steps including radiometric correction, atmospheric correction, and subsetting (clipping) to focus on the study area. LST is then derived from the thermal bands, and image classification is performed to identify different land cover types. Subsequently, LST classification and urban area analysis are carried out, followed by change detection to examine spatial and temporal trends. The final step involves analysis and verification to ensure the accuracy and reliability of the results.

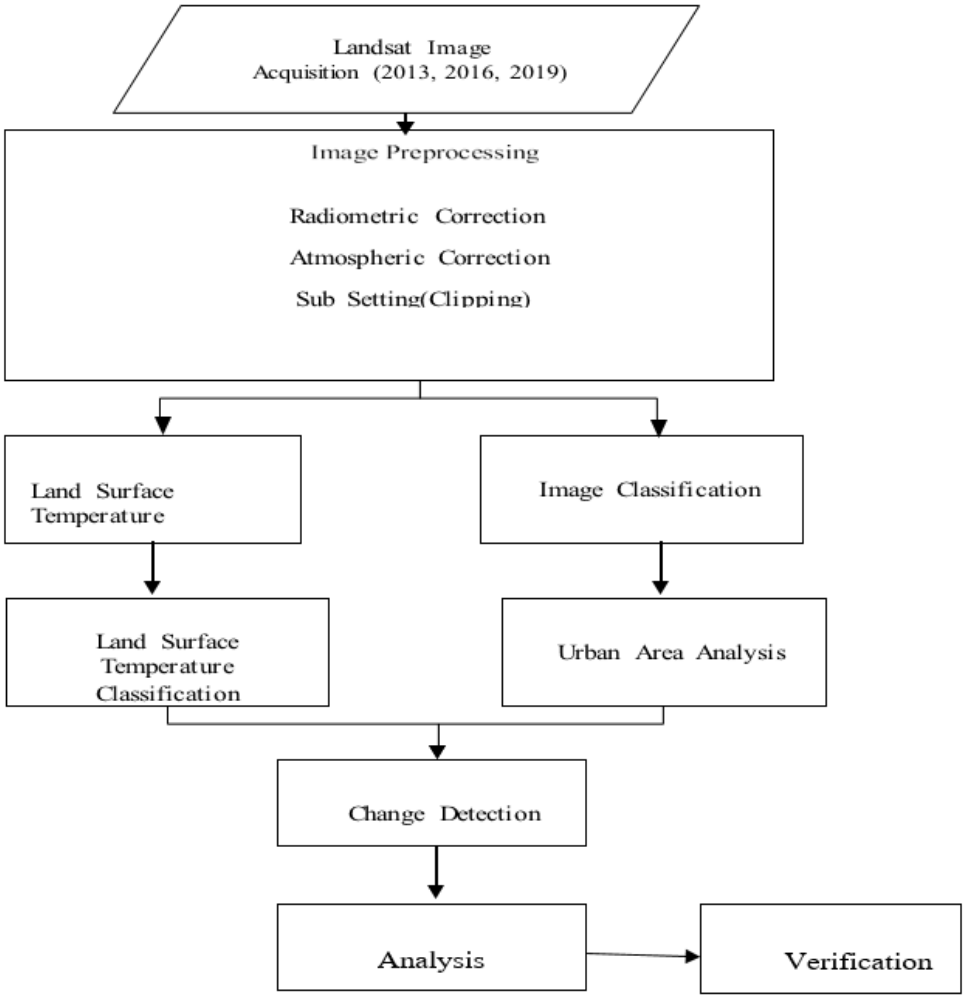

Figure 2. Workflow.

1.3 Data Source

The primary dataset for this research consists of Landsat 8 imagery from the Operational Land Imager (OLI) and Thermal Infrared Sensor (TIRS), Collection 1 Level-1 products, acquired on March 26, 2013; March 15, 2016; and January 3, 2019. Although more recent Landsat images (e.g., 2022, 2025) could provide updated information on land surface changes, this study focuses on the period 2013–2019 due to data availability and to maintain temporal consistency for trend analysis. Future research could incorporate more recent imagery to examine ongoing urban growth and LST dynamics.. These Landsat data can be freely accessed from the USGS portal and are processed by NASA to generate radiometric calibration and atmospheric correction algorithms for the Level-1 products. Landsat images are among the widely used satellite remote sensing data. Their spatial, spectral, and temporal resolution made them useful for mapping and planning projects (Wulder et al., 2019).

1.4 Radiometric Correction

Radiometric correction was applied to minimize errors in the satellite image's digital numbers (DN). This process enhances the quality and comparability of remotely sensed data, especially across multiple time periods (Chander et al., 2009). We used the empirical formula method for radiometric calibration. DN values were converted to Top-of-Atmosphere (TOA) reflectance using band-specific gain and bias values from the metadata:

$$TOA\ Reflectance = Gain * DN + Offset \quad (1)$$

After conversion, TOA reflectance was adjusted for solar elevation using band math with the following expression:

$$Corrected\ Reflectance = TOA\ Reflectance / \sin(44.34755968°) \quad (2)$$

1.5 Atmospheric Correction

Atmospheric correction removes the effects of the atmosphere to derive surface reflectance, improving image interpretability (Rumora et al., 2020). Accurate correction requires parameters like water vapor and aerosol distribution. Without such data, we used the Dark Object Subtraction (DOS) method, which assumes some pixels are in complete shadow and their radiance is due to atmospheric scattering. This path radiance is subtracted from all pixels. While less accurate, DOS is helpful when atmospheric data is unavailable.

1.6 Land Surface Temperature

Land surface temperature was retrieved from the thermal infrared band of Landsat images (band 10 of Landsat 8). The basic steps for the retrieval of LST are given below:

Conversion of pixel values to radiance:

The pixel values from digital number units were converted into radiance using the header file's parameters of Landsat images as follows:

$$L_\lambda = ML * QCAL + AL \quad (3)$$

This converts raw digital numbers (DN) from the satellite sensor into spectral radiance values, where ML represents the multiplicative rescaling factor, QCAL is the quantized calibrated pixel value, and AL is the additive rescaling factor, both obtained from the Landsat metadata file.

Atmospheric correction:

Removal of atmospheric effects from the thermal bands is essential to convert radiance to reflectance measures. Therefore, atmospheric correction uses the Dark Object Subtraction (DOS) Method.

Conversion of spectral radiance to at-sensor brightness temperature (BT):

Radiance values were then converted to at-sensor brightness temperature (in Celsius).

$$BT = \frac{K_2}{\ln\left(\frac{K_1}{L_\lambda} + 1\right)} - 273.15 \quad (4)$$

Here, – 273.15 is the Kelvin temperature constant.

Determination of Land Surface Emissivity (LSE):

Emissivity was estimated based on land cover type. The Portion of Vegetation (PV) is calculated as given in equation (5).

$$PV = \left(\frac{NDVI - NDVI_{\min}}{NDVI_{\max} - NDVI_{\min}}\right)^2 \quad (5)$$

$$LSE = 0.004 * PV + 0.986 \quad (6)$$

Land surface emissivity is calculated using the vegetation proportion, where the coefficients 0.004 and 0.986 are empirically derived constants that account for the emissivity characteristics of vegetated and non-vegetated surfaces.

Land Surface Temperature retrieval:

LST was calculated using the corrected brightness temperature and emissivity, applying the following formula:

$$LST = \frac{BT}{1 + \left(\lambda * \frac{BT}{C_2}\right) * \ln(LSE)} \quad (7)$$

Where, λ is the central band wavelength of emitted radiance (11.45 μm)

$$C_2 = \left(\frac{h * c}{\sigma}\right) = (1.438 * 10^{-2} mK) \quad (8)$$

with h is Planck's constant ($6.62*10^{-34}$ Js), c is the velocity of light ($2.998*10^8$ m/s) and σ is the Boltzmann constant ($1.38*10^{-23}$ J/K).

1.7 Image Classification

In image classification, we prefer supervised classification, which is a pixel-based approach. Since supervised classification has generally been recommended for evaluating segmentation results, and because classification accuracy is also believed to be highly dependent on the quality of segmentation (Liu & Xia, 2010). Hence, supervised classification was thought to lead to a more accurate classification of our project work (Maxwell et al., 2018). Similarly, this method uses the spectral signature defined in the satellite image (Talukdar et al., 2020).

1.8 Change Detection

The change detection approach is based on subtracting images acquired twice. This is performed on a pixel-by-pixel level to create the difference image. In the process, the pixel value is deducted from the initial and final images. Image differencing was used to detect urban changes in the images acquired in 2013, 2016, and 2019, specifically comparing the 2013 image.

2. RESULTS

2.1 Land Use Land Cover Change

Supervised maximum likelihood classification was applied to Landsat imagery to generate Land Use Land Cover (LULC) maps for 2013, 2016, and 2019 (Figures 3-5). The classification identified three primary land cover categories: urban areas, forest cover, and cultivated land. This categorization enabled systematic analysis of spatial and temporal changes associated with rapid urbanization in Kathmandu Valley.

The classified maps reveal distinct spatial patterns of land cover transformation. Urban areas are predominantly concentrated in the central valley floor, while forest cover remains largely distributed along the peripheral hills. Cultivated land occupies the intermediate zones between urban centers and forested hillsides. Over the six-year study period, a clear trend of urban expansion emerged, characterized by the conversion of both agricultural and forest lands into built-up areas.

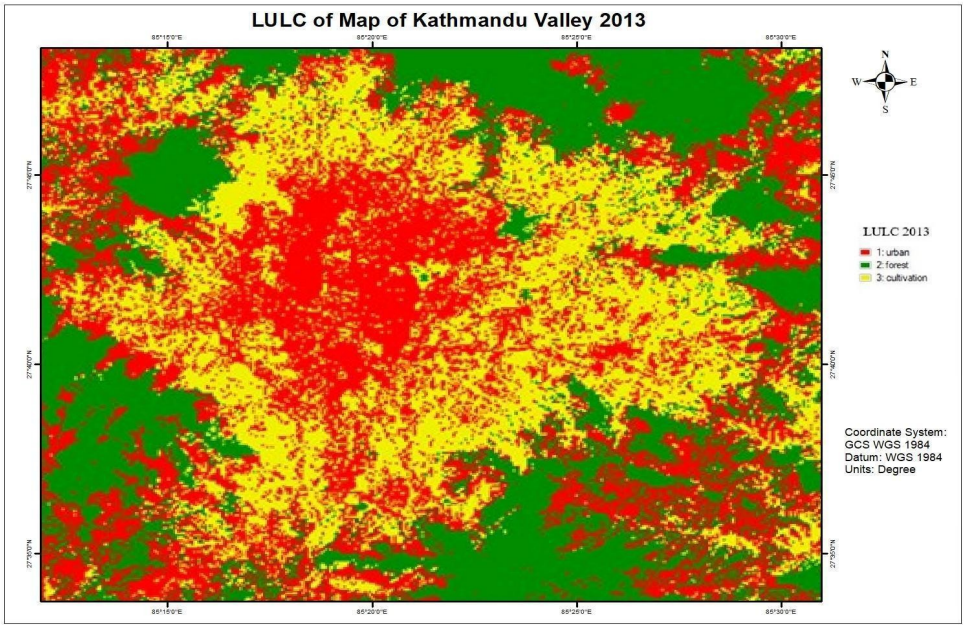

Figure 3. Supervised the Classification of Land Cover for analyzing the urban growth in 2013

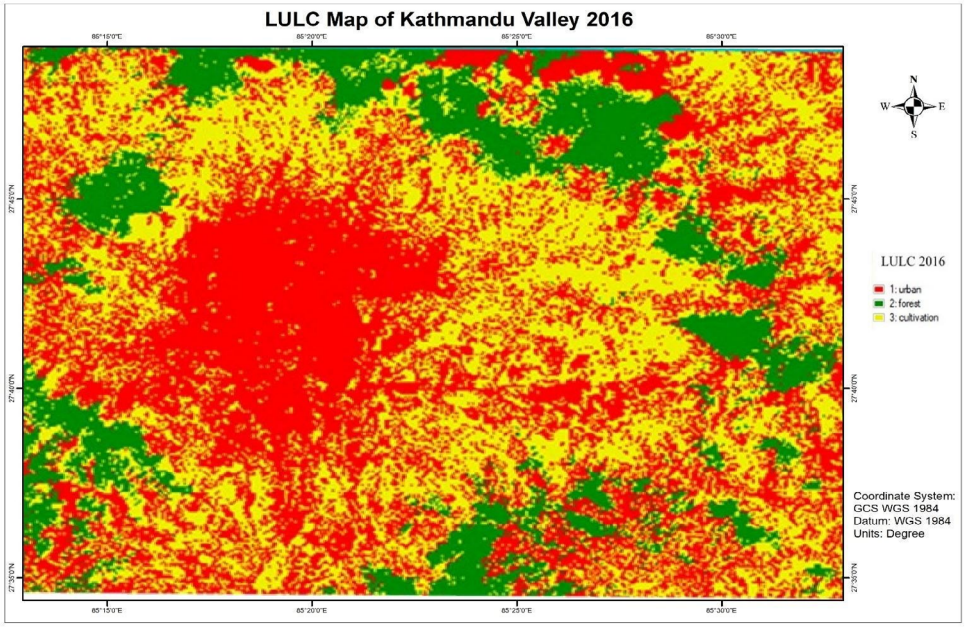

Figure 4. Supervised the Classification of Land Cover for analyzing the urban growth in 2016.

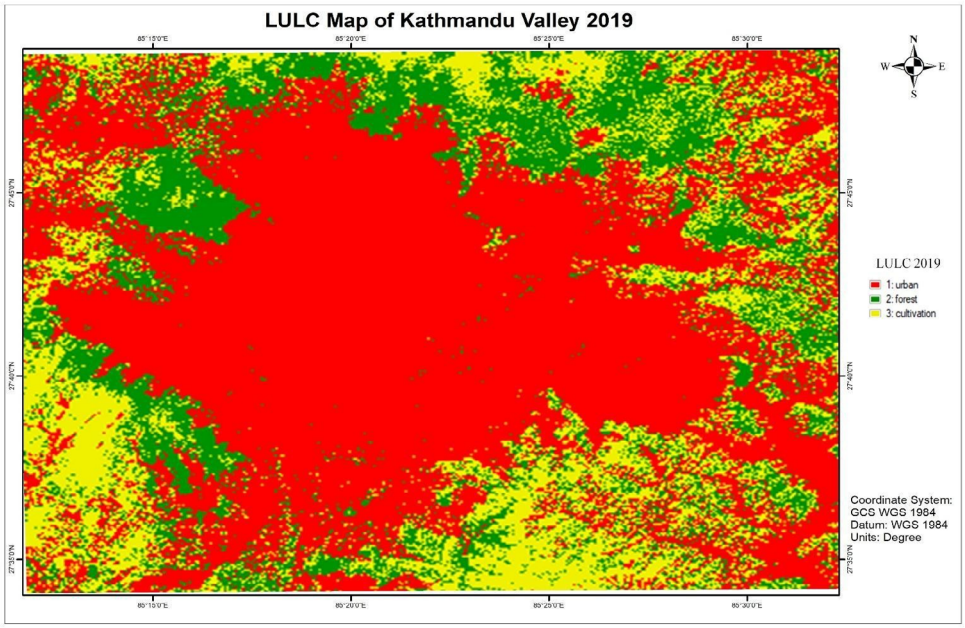

Figure 5. Supervised the Classification of Land Cover for analyzing the urban growth in 2019.

Table 1 presents the pixel count for each land cover class across the three time periods. The urban class showed a substantial increase from 681,405 pixels in 2013 to 1,026,126 pixels in 2019, representing approximately 50% growth. Conversely, forest cover declined dramatically from 650,982 pixels in 2013 to 339,749 pixels in 2016, though it showed partial recovery to 438,169 pixels by 2019. Cultivated land exhibited fluctuating trends, increasing from 572,177 pixels in 2013 to 745,718 pixels in 2016, before declining to 640,269 pixels in 2019.

Table 1. Total Pixels of Every Land Cover Class.

	2013	2016	2019
Urban	681405	819097	1026126
Forest	650982	339749	438169
Cultivation	572177	745718	640269

Table 2 translates these pixel counts into actual area coverage (in square meters), providing a more tangible understanding of landscape transformation. Urban areas expanded from 613.26 million m² in 2013 to 923.51 million m² in 2019, reflecting an increase of over 310 million m². Forest cover decreased from 585.88 million m² to 394.35 million m², representing a loss of approximately 191.53 million m² over the study period. Cultivated land increased initially to 671.15 million m² in 2016 but subsequently declined to 576.24 million m² by 2019.

Table 2. Total Area coverage of every land cover class.

	2013	2016	2019
Urban	613264500	737187300	923513400
Forest	585883800	305774100	394352100
Cultivation	514959300	671146200	576242100
Total	1714107600	1714107600	189410760

The percentage distribution of land cover classes (Table 3) provides critical insights into the proportional changes across the landscape. Urban areas increased from 35.78% of the total study area in 2013 to 48.76% in 2019, marking an increase of nearly 13 percentage points. This substantial growth came primarily at the expense of forest cover, which declined from 34.18% to 20.82%. Cultivated land maintained relatively stable coverage, varying between 30.04% and 30.42% across the study period, though it experienced intermediate fluctuations.

Table 3. Total percentage coverage of every land cover class.

	2013	2016	2019
Urban	35.7774798	43.0070609	48.75717726
Forest	34.1801063	17.8386759	20.8199418
Cultivation	30.0424139	39.1542631	30.42288094

2.2 Temporal Change Detection Statistics of Urban Growth

Change detection analysis was performed to quantify land cover transitions between the study periods. Tables 4 and 5 present the change statistics between 2013 and 2016, while Tables 6 and 7 show the changes between 2016 and 2019.

Table 4 presents the percentage change matrix for the 2013–2016 period. The matrix shows that 76.66% of urban areas remained stable, while 17.42% of new urban area came from forest conversion and 32.04% from cultivated land. Forest areas experienced significant transformation, with only 50.11% remaining as forest, and 49.90% undergoing class changes. Cultivated land showed 67.12% stability, with losses primarily to urban expansion. The image difference row indicates urban areas increased by 20.21%, forest decreased by 47.81%, and cultivated land increased by 30.33%.

Table 4. Percentage Change Statistics Table between years 2013-2016.

Percentage	Urban	Forest	Cultivation	Row Total	Class Total
Urban	76.661	17.418	32.042	100	100
Forest	1.291	50.105	0.834	100	100
Cultivation	22.048	32.477	67.123	100	100
Class Total	100	100	100	0	0
Class Changes	23.339	49.895	32.877	0	0
Image Difference	20.207	-47.81	30.33	0	0

Table 5 translates these percentages into actual area changes (in square meters) for 2013–2016. Urban areas expanded by 123.93 million m², growing from 613.26 million m² to 737.19 million m². This expansion occurred through the conversion of 102.05 million m² of forest and 165.00 million m² of cultivated land. Forest cover declined dramatically by 280.11 million m², decreasing from 585.88 million m² to 305.77 million m². Cultivated land showed a net increase of 156.19 million m², rising from 514.96 million m² to 671.15 million m².

Table 5. Area Change Statistics between years 2013-2016.

Area (sq. m)	Urban	Forest	Cultivation	Row Total	Class Total
Urban	470135700	102047400	165004200	737187300	737187300
Forest	7919100	293558400	4296600	305774100	305774100
Cultivation	135209700	190278000	345658500	671146200	671146200
Class Total	613264500	585883800	514959300	0	0
Class Changes	143128800	292325400	169300800	0	0
Image Difference	123922800	-280109700	156186900	0	0

Table 6 presents the percentage change matrix for the period 2016–2019. Urban areas maintained 64.04% stability, with 40.30% of new urban areas derived from cultivated land and a minimal contribution (0.31%) from forest. Forest areas exhibited only 35.58% stability, with 64.42% of the land undergoing class changes, while cultivated land had the lowest stability at 28.00%, with 72.00% of the land transitioning. The image difference indicates urban areas increased by 0.86%, forests increased by 28.97%, and cultivated land decreased by 14.14%.

Table 6. Percentage Change Statistics Table between years 2016-2019.

	Urban	Forest	Cultivation	Row Total	Class Total
Urban	64.039	0.31	40.301	100	100
Forest	9.88	35.58	31.695	100	100
Cultivation	26.081	64.111	28.003	100	100
Class Total	100	100	100	0	0
Class Changes	35.961	64.42	71.997	0	0
Image Difference	0.858	28.968	-14.141	0	0

Table 7 presents the area-based change statistics for 2016–2019. Urban areas expanded by 186.32 million m², increasing from 737.19 million m² to 923.51 million m². This growth primarily came from cultivated land conversion (270.48 million m²). Forest cover increased by 88.58 million m², rising from 305.77 million m² to 394.35 million m², largely through conversion from cultivated areas (196.03 million m²). Cultivated land declined by 94.90 million m², decreasing from 671.15 million m² to 576.24 million m².

Table 7. Area Change Statistics between years 2016-2019.

Area (sq. m)	Urban	Forest	Cultivation	Row Total	Class Total
Urban	472086000	946800	270480600	743513400	743513400
Forest	72837000	108792900	212722200	394352100	394352100
Cultivation	192264300	196034400	187943400	576242100	576242100
Class Total	737187300	305774100	671146200	0	0
Class Changes	265101300	196981200	483202800	0	0
Image difference	6326100	88578000	-94904100	0	0

Overall, the change detection analysis reveals that urban areas expanded by approximately 310.25 million m² between 2013 and 2019, with cultivated land serving as the primary source of urban expansion throughout the study period. Forest cover showed a net decline of 191.53 million m² despite the partial recovery in the later period.

The urban growth graph for the study area's time periods is illustrated in Figure 6. The graph shows us that the urban growth is gradually increasing. The temporal LULC trend, illustrated in Figure 6, demonstrates a consistent upward trajectory of urban growth over the six-year study period. The data clearly reveal that urbanization has been the dominant driver of land transformation, often occurring at the expense of forest and agricultural lands. This pattern suggests unplanned urban sprawl and underscores the urgent need for effective land-use management strategies to ensure sustainable urban development.

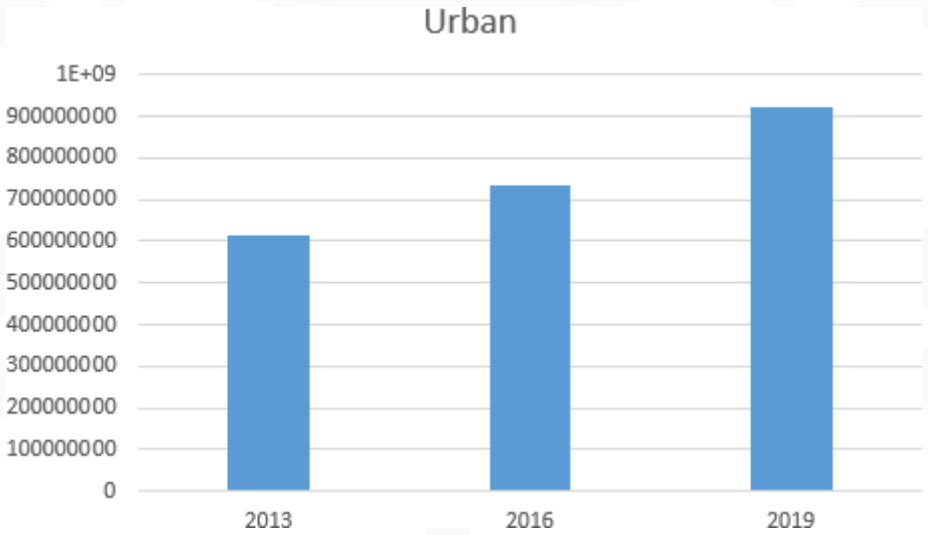

Figure 6. Chart of total area coverage by urban growth.

3. MITIGATION STRATEGIES

To mitigate the impacts of rapid urban growth and rising land surface temperatures in Kathmandu Valley, targeted actions are needed. Expanding green spaces through tree planting along the Ring Road, major city areas, and dense neighborhoods, as well as promoting green roofs can reduce heat buildup. Cool roofs in industrial zones, light pavements in public spaces, and reflective facades in new residential areas should be encouraged. Integrating climate-responsive architecture that blends traditional Nepali design with modern passive cooling can further reduce heat stress. Strengthened public awareness, community involvement, and strict enforcement of planning and building codes are also vital for effective heat mitigation in the Valley.

The implementation of these mitigation strategies requires coordinated efforts from government agencies, municipal authorities, private developers, and citizens. While individual measures provide benefits, the synergistic effect of combined strategies would be most effective in addressing the urban warming challenge. Given the rapid pace of urbanization documented in this study, immediate action is imperative to ensure a sustainable and livable future for Kathmandu Valley.

4. DISCUSSION

4.1 Land Surface Temperature

The LST maps of the study area in 2013, 2016, and 2019 are shown below. LST ranged from -3.270°C to 36.460°C in 2013, -1.91°C to 27.030°C in 2016, and 13.260°C to 40.840°C in 2019. The maximum temperature declined sharply in the year 2016 by around 90°C. However, the minimum temperature has been increasing in subsequent years. There is a sudden decline in the maximum temperature from 2013 to 2016, as some days of the year in the past could have been hotter, despite the influence of the urban warming phenomenon caused by urban growth over time. LST pattern analysis indicates a low temperature, represented by a blue tone, at the edges of all maps, which corresponds to the forest area. The yellow patch in the middle represents the urban settlements, and the red patches at the edges represent bare soil and even rocks in the high cliffs. A similar trend was observed in studies conducted by Tran et al. (2017)

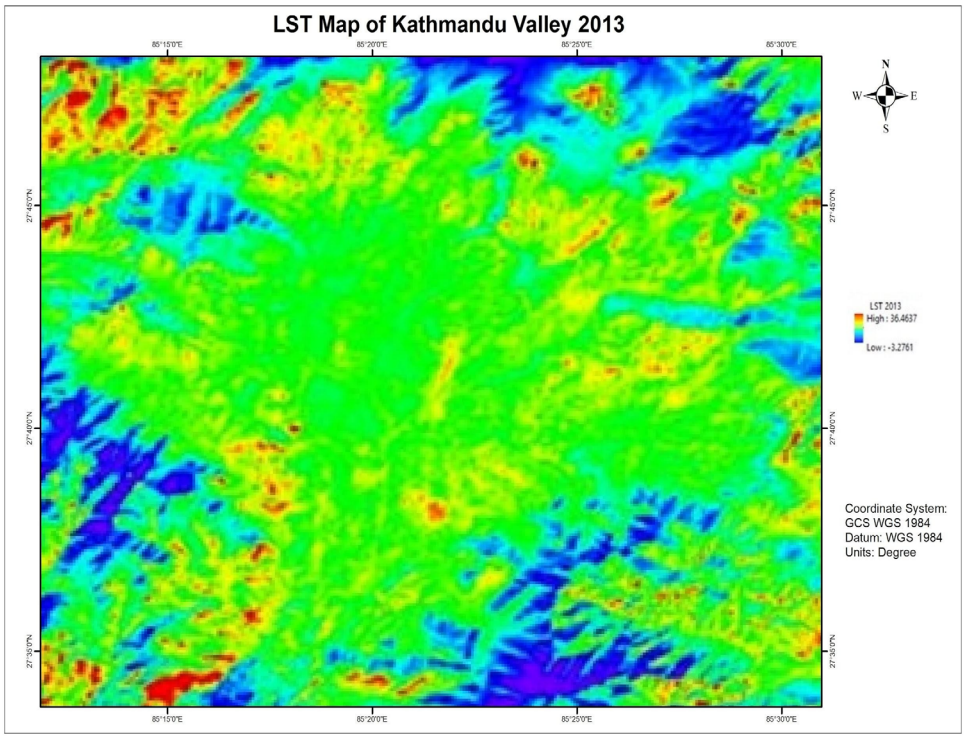

Figure 7. LST of Kathmandu of the years 2013.

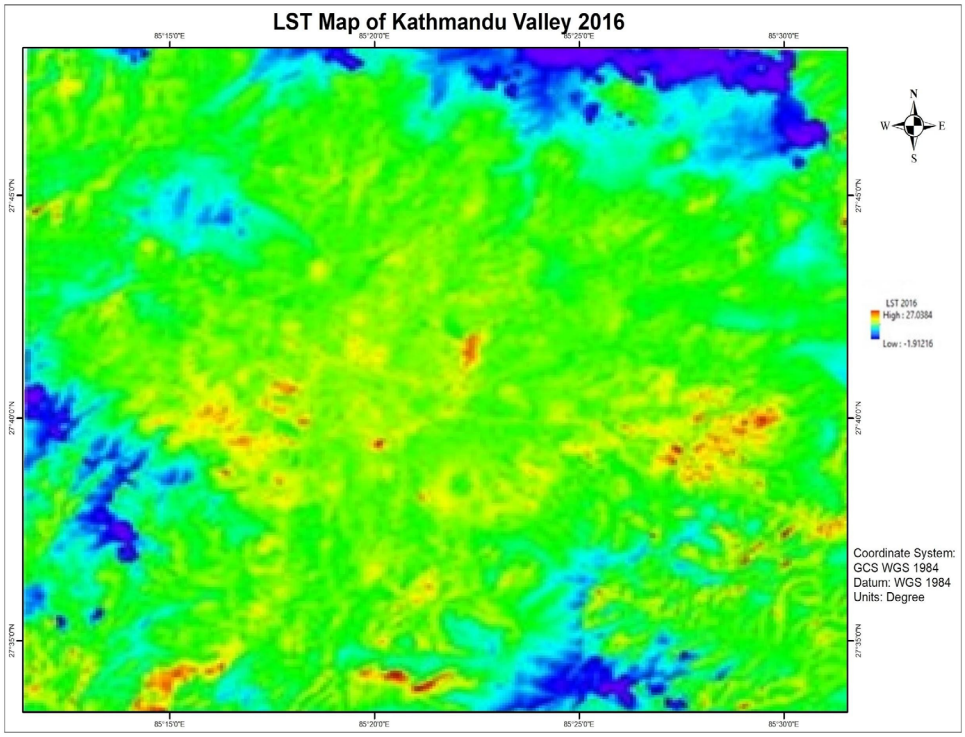

Figure 8. LST of Kathmandu of the years 2016.

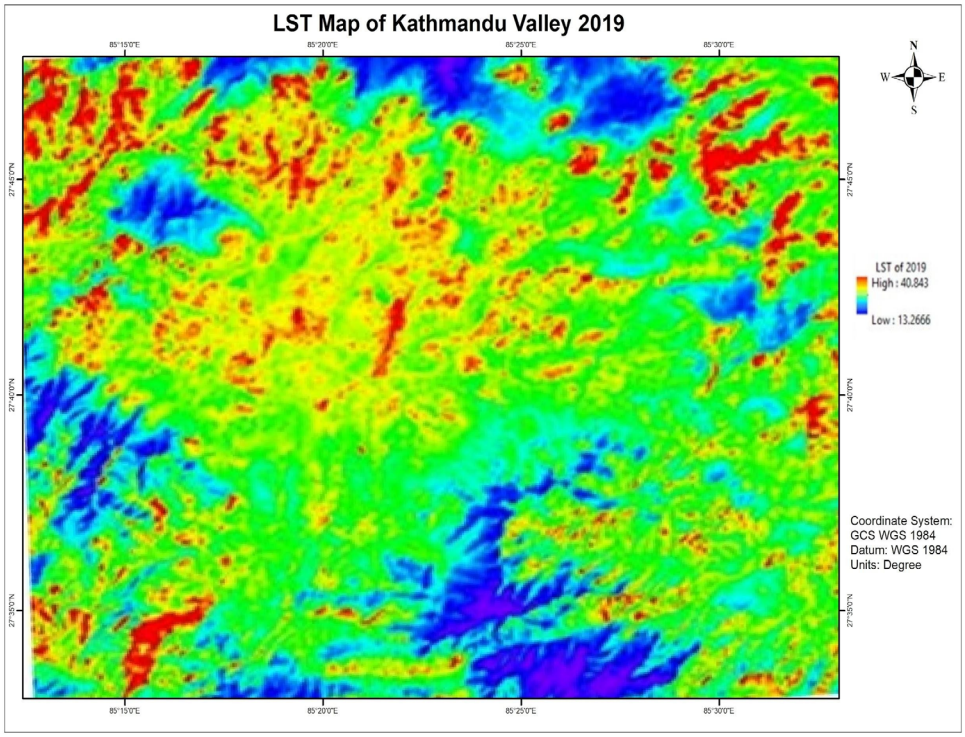

Figure 9. LST of Kathmandu of the years 2019.

Extreme fluctuations in temperature that were observed between 2013 and 2016 in this paper may have been driven by seasonal or meteorological conditions, a factor also noted by Rani et al. (2021) with respect to the temporal stability of Land Surface Temperature (LST). The observed spatial temperature distribution, which was cooler on the vegetated perimeter and hotter in the urban core, corresponds with recent research on the Urban Heat Island (UHI) effect in Kathmandu Valley. For example, Khatri et al. (2025) also documented an intense and intensifying UHI effect in the valley, linking land surface temperature increases directly with the expansion of built-up areas. Additionally, the distinct differences in LST that were observed based on land cover (i.e., built-up areas and bare soil having the highest) is consistent with the scientific literature on global land and the thermal properties of landscapes and other articles such as Guha et al. (2021). These comparisons reinforce that the dynamics of LST in the Kathmandu Valley configuration reflect localized urban expansion within the larger scope of globally observed climate patterns.

CONCLUSIONS

The study revealed a high rate of urban growth in the Kathmandu valley. The primary drivers of such growth are high population influx and inadequate land use planning. As a result, productive agricultural land and open areas are being replaced by concrete structures. This trend will become more severe unless proper land-use plans and policies are implemented. Based on our analysis of the thermal pattern of the study area over the given period, we found a gradual increase in temperature in the urban area. The study proved that the surface temperature is influenced by urban growth. However, the study had some limitations. The resolution of the images was just moderate for classification and change detection purposes. Despite a massive repository of Landsat imagery, it can sometimes be challenging to find suitable photos that meet our requirements.

Hence, we recommend that, as urban growth in the Kathmandu Valley is in a critical condition, it is high time that concerned authorities take necessary initiatives and that urban residents develop resilience to urban growth. We also recommend using high-resolution images and other classification methods to accurately classify land cover to detect urban development in the area.

REFERENCES

Akher, S. K., & Chattopadhyay, S. (2017). Impact of urbanization on land surface temperature-a case study of Kolkata New Town. Int J Eng Sci, 6(1), 71-81. https://doi.org/10.9790/1813-0601027181

Bhattarai, R., Alifu, H., Maitiniyazi, A., & Kondoh, A. (2017). Detection of land subsidence in Kathmandu Valley, Nepal, using DInSAR technique. Land, 6(2), 39. https://doi.org/10.3390/LAND6020039

Chander, G., Markham, B. L., & Helder, D. L. (2009). Summary of current radiometric calibration coefficients for Landsat MSS, TM, ETM+, and EO-1 ALI sensors. Remote sensing of environment, 113(5), 893-903. https://doi.org/10.1016/j.rse.2009.01.007

Guha, S., Govil, H., & Gill, N. (2021). A case study on the relationship between land surface temperature and land use/land cover over Bhubaneswar, India. Geology, Ecology, and Landscapes, 5(3), 218–228. https://doi.org/10.1080/24749508.2020.1757535

Hulley, G. C., Ghent, D., Göttsche, F. M., Guillevic, P. C., Mildrexler, D. J., & Coll, C. (2019). Land surface temperature. In Taking the Temperature of the Earth: Steps towards Integrated Understanding of Variability and Change (pp. 57–127). Elsevier. https://doi.org/10.1016/B978-0-12-814458-9.00003-4

Inu Pradhan Salike, L. F. (2015). Kathmandu Valley, Nepal: Climate Change Vulnerability Assessment.

Ishtiaque, A., Shrestha, M., & Chhetri, N. (2017). Rapid urban growth in the Kathmandu Valley, Nepal: Monitoring land use land cover dynamics of a himalayan city with landsat imageries. Environments, 4(4), 72. https://doi.org/10.3390/ENVIRONMENTS4040072

Joshi, D. R. (2023). Urbanization trend in Nepal. Contemporary Research: An Interdisciplinary Academic Journal, 6(1), 51-62. https://doi.org/10.3126/craiaj.v6i1.55367

K.C., B., & Shepherd, J. M. (2015). A study of urban heat island intensity in Kathmandu Valley, Nepal [Abstract]. AGU Fall Meeting Abstracts.

Khatri, B., & Khatri, R. (2024). Assessment on the relationship of spectral indices with land surface temperature using Google Earth Engine: A case study of Chitwan District, Nepal. Advances in Geomatics, 2(2), 74–87. https://doi.org/10.5281/zenodo.14555495

Khatri, B., Kharel, B., Dhakal, P., Acharya, S., & Thapa, U. (2025). Spatio-temporal dynamics of urban heat island using Google Earth Engine: Assessment and prediction—A case study of Kathmandu Valley, Nepal. Climate Services, 38, 100560. https://doi.org/10.1016/j.cliser.2025.100560

Liu, D., & Xia, F. (2010). Assessing object-based classification: advantages and limitations. Remote Sensing Letters, 1(4), 187–194. https://doi.org/10.1080/01431161003743173

Maxwell, A. E., Warner, T. A., & Fang, F. (2018). Implementation of machine-learning classification in remote sensing: An applied review. International Journal of Remote Sensing, 39(9), 2784–2817. https://doi.org/10.1080/01431161.2018.1433343

Rani, M., Kumar, P., Pandey, P. C., Srivastava, P. K., Chaudhary, B. S., Tomar, V., & Mandal, V. P. (2021). Multi-temporal NDVI and surface temperature analysis for Urban Heat Island impact assessment of Varanasi City, India. Quaternary International, 575-576, 249–259. https://doi.org/10.1016/j.quaint.2020.07.046

Rimal, B., Zhang, L., Keshtkar, H., Haack, B. N., Rijal, S., & Zhang, P. (2018). Land use/land cover dynamics and modeling of urban land expansion by the integration of cellular automata and markov chain. ISPRS International Journal of Geo-Information, 7(4), 154. https://doi.org/10.3390/ijgi7040154

Rumora, L., Miler, M., & Medak, D. (2020). Impact of various atmospheric corrections on sentinel-2 land cover classification accuracy using machine learning classifiers. ISPRS International Journal of Geo-Information, 9(4), 277. https://doi.org/10.3390/IJGI9040277

Talukdar, S., Singha, P., Mahato, S., Pal, S., Liou, Y. A., & Rahman, A. (2020). Land-use land-cover classification by machine learning classifiers for satellite observations—A review. Remote sensing, 12(7), 1135. https://doi.org/10.3390/rs12071135

Thapa, R. B., & Murayama, Y. (2012). Scenario based urban growth allocation in Kathmandu Valley, Nepal. Landscape and Urban Planning, 105(1-2), 140-148. https://doi.org/10.1016/j.landurbplan.2011.12.007

Timsina, N. P., Shrestha, A., Poudel, D. P. & Upadhyaya, R. (2020). Trend of urban growth in Nepal with a focus in Kathmandu Valley: A review of processes and drivers of change. https://doi.org/10.7488/ERA/722

Tran, D. X., Pla, F., Latorre-Carmona, P., Myint, S. W., Caetano, M., & Kieu, H. V. (2017). Characterizing the relationship between land use land cover change and land surface temperature. ISPRS Journal of Photogrammetry and Remote Sensing, 124, 119-132. https://doi.org/10.1016/J.ISPRSJPRS.2017.01.001

Wulder, M. A., Loveland, T. R., Roy, D. P., Crawford, C. J., Masek, J. G., Woodcock, C. E., Allen, R. G., Anderson, M. C., Belward, A. S., Cohen, W. B., Dwyer, J., Erb, A., Gao, F., Griffiths, P., Helder, D., Hermosilla, T., Hipple, J. D., Hostert, P., Hughes, M. J., … Zhu, Z. (2019). Current status of Landsat program, science, and applications. Remote Sensing of Environment, 225, 127–147. https://doi.org/10.1016/j.rse.2019.02.015